

---

# Q-Tacit: Image Quality Assessment via Latent Visual Reasoning

---

Yuxuan Jiang<sup>1,†</sup>, Yixuan Li<sup>1,†,✉</sup>, Hanwei Zhu<sup>2</sup>, Siyue Teng<sup>1</sup>, Fan Zhang<sup>1</sup>, David Bull<sup>1</sup>

<sup>1</sup> Visual Information Lab, University of Bristol

<sup>2</sup> Nanyang Technological University

{yuxuan.jiang, siyue.teng, fan.zhang, dave.bull}@bristol.ac.uk

yixuanli423@gmail.com

hanwei.zhu@ntu.edu.sg

<https://github.com/YuxuanJJ/Q-Tacit>

## Abstract

Vision-Language Model (VLM)-based image quality assessment (IQA) has been significantly advanced by incorporating Chain-of-Thought (CoT) reasoning. Recent work has refined image quality reasoning by applying reinforcement learning (RL) and leveraging active visual tools. However, such strategies are typically language-centric, with visual information being treated as static preconditions. Quality-related visual cues often cannot be abstracted into text in extenso due to the gap between discrete textual tokens and quality perception space, which in turn restricts the reasoning effectiveness for visually intensive IQA tasks. In this paper, we revisit this by asking the question, “*Is natural language the ideal space for quality reasoning?*” and, as a consequence, we propose **Q-Tacit**, a new paradigm that elicits VLMs to reason beyond natural language in the latent quality space. Our approach follows a synergistic two-stage process: (i) injecting structural visual quality priors into the latent space, and (ii) calibrating latent reasoning trajectories to improve quality assessment ability. Extensive experiments demonstrate that **Q-Tacit** can effectively perform quality reasoning with significantly fewer tokens than previous reasoning-based methods, while achieving strong overall performance. This paper validates the proposition that language is not the only compact representation suitable for visual quality, opening possibilities for further exploration of effective latent reasoning paradigms for IQA. Source code will be released to support future research.

## 1 Introduction

Image quality assessment (IQA) plays an essential role in modern computer vision [25, 58, 56, 75, 48], attempting to establish a quantitative mapping between a digital image and its human subjective evaluation. Echoing Moravec’s paradox [36], *it is comparatively easy to make computers exhibit adult-level performance on intelligence tests, while difficult to give them the perception of a one-year-old*, IQA is instinctive to humans, yet requires complex reasoning to create accurate objective measures.

No-Reference (NR) IQA, which assesses images without a reference, has evolved for decades from knowledge-driven [34, 35] to data-driven approaches [46, 20], tackling generalization [74, 5, 7], active fine-tuning [53], and continual adaptation [69] problems. Despite these advances, such methods

---

<sup>†</sup>Equal contribution.

<sup>✉</sup>Corresponding authors

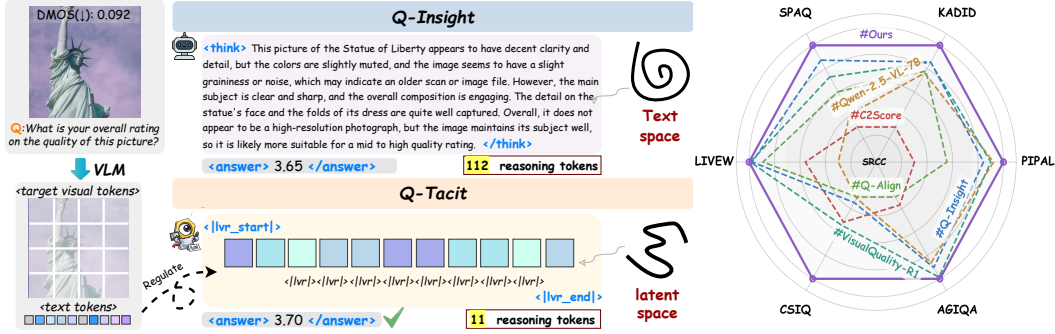


Figure 1: **Motivation and overview of Q-Tacit.** We compare **Q-Tacit** and Q-Insight [25], which perform quality reasoning in a latent space and a text space, respectively. `<|lvr_start|>` and `<|lvr_end|>` encapsulate the latent reasoning process, and `<|lvr|>` is a placeholder for a latent slot token that allocates one latent reasoning step. **Q-Tacit** excels at image quality scoring on out-of-distribution datasets (Right) while requiring only 10% visible token counts compared to Q-Insight (Left).

remain easily challenged by out-of-distribution (OOD) scenarios. Their inference primarily depends on the implicit function of the learned representation, which can lack delicate reasoning<sup>1</sup> for more reliable quality inference.

Building upon the rapid advancement of large Visual Language Models (VLMs), NR-IQA has leveraged their extensive visual reasoning abilities and cross-modal semantic contextualization for quality evaluation [45, 66, 67, 72, 1]. Pre-existing VLM-based methods generally fall into two categories: methods without explicit reasoning, such as Q-Align [56], Compare2Score [75] and DeQA-Score [63], and reasoning-induced methods, represented by VisualQuality-R1 [58], Q-Insight [25], and Q-ponder [4]. Amongst these categories, reasoning-induced methods have recently attracted increased attention. Compared to direct inference, these methods usually introduce intermediate rationales as the reasoning route to quality scores. As shown in Fig. 1, when evaluating an input image, Q-Insight first describes quality-relevant visual cues in natural language, providing additional backing for subsequent quality scoring. In [71], it is demonstrated that aligning images to the Reinforcement Learning (RL)-derived quality-description text space can preserve generalization without reasoning at inference, further suggesting that the improved reasoning signal can accordingly boost quality prediction. Therefore, if quality-awareness can be enhanced by refining the reasoning process, the explicit form of the intermediate process becomes pivotal. Although text-centric reasoning provides certain explainability for IQA, it can be difficult for these methods to faithfully form quality abstractions that go beyond what can be easily verbalized [22, 24, 51]. This naturally leads to the following question: *is natural language the ideal space for visual quality reasoning?*

In this paper, we explore the potential of extending VLM quality reasoning beyond text towards the use of visual tokens that directly encode quality information. Rather than improving a model’s ability to verbalize image quality in natural language, we instead drive it to reason in a latent quality space shared by continuous visual tokens and discrete text tokens [22, 38]. A related line of research seeks to enforce stronger visual grounding in quality-assessment reasoning via active tools, such as zooming in [26]. Although such tools can partially compensate for the loss of visual quality details caused by VLMs’ cross-modality bias and interference [68, 3], they still revert to refining text generation, and thus the fundamental gap persists between images and textual trajectories. Hence, we adopt latent visual reasoning (LVR) [22], a multimodal reasoning scheme that moves reasoning towards a latent quality space, encoding visual semantics relevant to both the input image and the query. LVR has been effective in tasks such as object detection [51] and image generation [8]. By exploring reasoning interfaces that couple more tightly with perceptual evidence, VLMs can benefit in three main ways: (i) improved generalization via visually grounded latent reasoning space; (ii) no reliance on dense textual supervision; and (iii) efficient reasoning that requires a significantly lower token budget.

<sup>1</sup>In line with the prevalent usage in VLM research, “reasoning” here denotes an inspectable explicit inference trace that links vision to model outputs.

Specifically, we propose **Q-Tacit** to steer VLMs to reason about image quality in the latent quality space. We instantiate a dedicated reasoning space by inserting a sequence of latent tokens, and formulate it as latent-space visual reconstruction. Instead of using visual embeddings as static conditioning, the model performs a series of auto-regressive hidden-state transitions over the latent tokens to reason with query-relevant visual tokens before outputting a final prediction, as shown in Fig. 1. Such transitions can be regarded as continuous *latent visual thoughts* towards quality, similar to Chain-of-Thought (CoT) in textual space [22, 24, 51]. Finally, we calibrate the reasoning trajectories in this latent space, which enables the model to operate directly on continuous perceptual representation, thereby preserving subtle cues to reason out the quality score. Practically, we realize this scheme by introducing a synergistic two-stage process elaborated as follows:

*Stage I: Latent Prior Injection.* We form a latent quality space and teach the model basic latent reasoning patterns through Supervised Fine-Tuning (SFT). We propose to use the Regions of Interest (ROI)-based quality data to supervise the last hidden states and force latent tokens to reconstruct quality-relevant visual evidence, thereby linking latent reconstruction and perceptual scoring.

*Stage II: Quality-aligned Calibration.* We then perform the latent Group Relative Policy Optimization (GRPO) algorithm [43, 15] to calibrate latent reasoning trajectories towards human quality perception. We design a gaussian-based dense quality scoring reward and combine it with a format-compliance reward to jointly optimize quality reasoning without requiring dense manual annotations.

As shown in Fig. 1, our Q-Tacit exhibits remarkable quality prediction performance on OOD datasets while demanding significantly reduced reasoning tokens. Our empirical results further reveal that the latent space compactly encodes quality-relevant evidence by tightly coupling reasoning embeddings with visual embeddings, leading to a reasoning space that is more sensitive to subtle local degradations. Our contributions are three-fold:

- We propose **Q-Tacit**, the first reasoning-induced IQA framework in the latent space. Distinguished from previous methods which conduct text-centric quality reasoning, our approach achieves superior quality prediction performance in the latent visual space with incremental reasoning token saving.
- We introduce a continuous latent space framed by latent evidence reconstruction and aggregation, which embeds quality-relevant perception and general visual understanding simultaneously. This enables effective and scalable image quality reasoning towards human perception.
- We conduct extensive experiments to validate the effectiveness of reasoning quality in the latent space. Q-Tacit exhibits consistent improvements on quality prediction compared with previous methods across diversified distortions.

## 2 Related Work

### 2.1 Image Quality Assessment Methods

**IQA without explicit reasoning** learns an implicit function that directly maps image representations to quality levels without exposing intermediate decision steps. From early NR-IQA pipelines [34, 35] that rely on hand-crafted statistics, such as BRISQUE [34], to modern deep learning methods [2, 46, 20], most approaches still follow the same paradigm: extract a global representation and output a scalar quality score. In this sense, the reasoning process is implicitly manifested by model parameters. With the emergence of VLMs [29, 1], some attempts have been made to bias the model toward following image quality assessment instructions via Supervised Fine-Tuning (SFT), and then directly output quality ratings [55, 56, 75, 65, 63, 64]. For example, Q-Align [56], Compare2Score [75], and DeQA-Score [63] tweak VLMs with sophisticatedly designed quality prompting schemes and achieve significant progress. Such direct scoring is attractive because of its scalability, but limits generalization under distribution shifts.

**IQA with explicit reasoning** encourages the model to decompose complex evaluation tasks into sequential sub-steps. With the emergence of CoT [54] and its variants [52, 73, 62], it has become clear that eliciting intermediate steps can impose a positive influence on large models. This motivates a shift from purely score regression to approaches that explicitly verbalize the quality assessment process [55, 25, 58], yielding more explainable IQA outputs. Existing efforts can be classified into three categories based on how reasoning is induced: (i) SFT, such as Q-Instruct [55], Co-Instruct [57], and Depict-QA [65]; (ii) RL, e.g., Q-Insight [25], VQ-Insight [70], VisualQuality-R1 [58] and Q-

Ponder [4]; and (iii) active visual tools, including ZoomIQA [26] and Q-Probe [4]. Despite these advances in both reasoning and scoring, the reasoning trajectories predominantly anchor to the textual space. However, representing continuous visual signals via discrete text tokens can entail reductive abstraction [22, 38, 32], which could limit reasoning efficacy in visual tasks.

## 2.2 Visual Reasoning in VLMs

Visual reasoning refers to performing compositional inference grounded in vision to derive answers beyond direct recognition [30]. Early progress has largely been text-centric, with methods such as CoT prompting [54], and RL-induced models like Vision-R1 [19] and Visual-RFT [30] — all of which primarily improve visual question answering by eliciting better textual reasoning traces over fixed visual embeddings. More recent work moves toward interleaved multimodal reasoning by generating visual representations for reasoning steps [61, 38] or reintegrating specific visual tokens into reasoning [6]. Collectively, these advances aim to enhance the visual awareness of reasoning. A parallel line of work in natural language processing has attempted to explore reasoning in a latent space rather than directly in the token space [44, 10]. COCONUT [16] regards hidden states as continuous thoughts to be fed back to the model iteratively, while [13] uses pause tokens to allocate extra internal computation without generating visible tokens. More recent approaches have begun to explore latent-space reasoning in VLMs [22, 24, 51]. These demonstrate that latent representations can act as an effective reasoning space. Distinctly, **Q-Tacit** is the first work to explore IQA in the latent reasoning space by employing a synergistic two-stage strategy.

## 3 Methodology

### 3.1 Preliminaries

**VLM as token-conditioned decoding.** Given an image  $x$ , a visual encoder  $E_v(\cdot)$  produces visual features that are projected into the LLM embedding space via a projector  $P(\cdot)$ , yielding visual tokens  $V = \{v_j\}_{j=1}^N = P(E_v(x))$ . A conventional VLM then performs autoregressive decoding over a discrete vocabulary conditioned on  $V$  and the textual prompt.

**Latent visual reasoning.** [22] extends decoding with latent segments that alternate with standard text generation. Upon emitting a trigger `<|lvr_start|>`, the model pauses textual decoding and enters a latent mode, producing a sequence of continuous hidden states  $\mathcal{H}_{\text{latent}} = \{h_t\}_{t=1}^T$ , where  $T$  is the number of hidden-state involved. After the latent segment, the model emits `<|lvr_end|>` and resumes standard decoding.

**1) Supervising latent states with visual-token reconstruction.** To ground latent thoughts,  $\mathcal{H}_{\text{latent}}$  is supervised to reconstruct a set of target visual tokens. Let  $\mathcal{I}$  denote indices of visual tokens among ROIs, and let  $\phi(\cdot)$  map each  $i \in \mathcal{I}$  to a latent step  $\phi(i) \in \{1, \dots, T\}$ . To this end, the MSE loss is employed to optimize the latent reconstruction:

$$\mathcal{L}_{\text{LVR}} = \frac{1}{|\mathcal{I}|} \sum_{i \in \mathcal{I}} \|g(h_{\phi(i)}) - v_i\|_2^2, \quad (1)$$

where  $g(\cdot)$  projects hidden states to the visual-token space. During this process, the model is jointly optimized by the next-token prediction  $\mathcal{L}_{\text{NTP}}$  and latent visual reconstruction.

$$\mathcal{L}_{\text{SFT}} = \mathcal{L}_{\text{NTP}} + \lambda_{\text{lvr}} \mathcal{L}_{\text{LVR}}. \quad (2)$$

Specifically, the standard cross-entropy loss for next-token prediction is adopted only on the discrete outputs, and the latent reconstruction loss aligns predicted latent states with target visual embeddings.

**2) Latent GRPO.** Since the latent segment does not yield token log-probabilities and is treated as an internal continuous computation that conditions generation, GRPO is applied only to discrete output tokens. Concretely, for each rollout, realized latent states  $\hat{\mathcal{H}}_{\text{latent}}$  inside the latent space are recorded and replayed to restore an identical conditioning context. Let  $y = \{y_t\}_{t \in \mathcal{T}_{\text{text}}}$  denote the sequence of discrete response tokens, where  $\mathcal{T}_{\text{text}}$  is the index set of token-decoding steps (excluding latent steps) and define  $T_y = |\mathcal{T}_{\text{text}}|$  as the number of discrete response tokens. The token importance

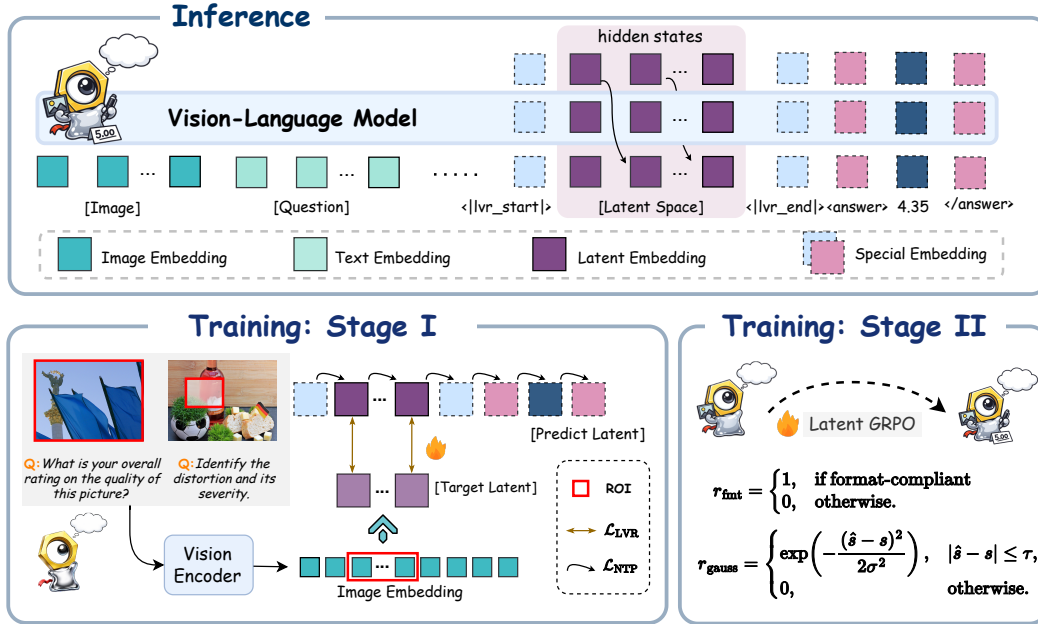


Figure 2: **Overview of Q-Tacit.** We introduce a compact latent quality-reasoning segment wrapped by special tokens  $\langle |lvr\_start| \rangle$  and  $\langle |lvr\_end| \rangle$ , where the model propagates latent embeddings (i.e., internal hidden states) as a compact quality space instead of generating textual rationales. Then directly outputs the final quality score in  $\langle answer \rangle$  and  $\langle /answer \rangle$  when a stopping criterion is met.

ratio  $r_t(\theta)$  under the updated policy  $\pi_\theta$  and the rollout policy  $\pi_{old}$  can be written as,

$$r_t(\theta) = \frac{\pi_\theta(y_t | x, \hat{\mathcal{H}}_{latent}, y_{<t})}{\pi_{old}(y_t | x, \hat{\mathcal{H}}_{latent}, y_{<t})}. \quad (3)$$

The latent segment is treated as a fixed conditioning context. For each input, we sample a group of  $K$  rollouts and optimize:

$$\mathcal{J}(\theta) = \mathbb{E} \left[ \frac{1}{K} \sum_{k=1}^K \sum_t \min(r_t(\theta) \hat{A}_t, \text{clip}(r_t(\theta), 1 - \epsilon, 1 + \epsilon) \hat{A}_t) \right] - \beta \sum_t D_{KL}(\pi_\theta || \pi_{ref}), \quad (4)$$

where  $\hat{A}_t$  denotes the group-relative advantages,  $\pi_{ref}$  is the SFT reference model,  $\epsilon$  is the clipping range, and  $\beta$  is the Kullback–Leibler (KL) coefficient.

### 3.2 The Q-Tacit Framework

**Q-Tacit** is a reasoning-induced NR-IQA framework that functions in the latent space. As illustrated in Fig. 2, Q-Tacit first learns a latent quality space and latent reasoning patterns via LVR-induced SFT (Section 3.2.1), which are consistently invoked during inference. Next, the reasoning trajectories are calibrated within the latent space via latent GRPO to better assess image quality (Section 3.2.2). We finally elaborate on the data formulation for the two training stages (Section 3.3). Fig. 2 shows the latent-reasoning based two-stage paradigm of Q-Tacit, and the details are elaborated below.

#### 3.2.1 Stage I: Latent Prior Injection via SFT

The main objective of this stage is to form a latent quality space and teach the model basic latent reasoning patterns, including when to invoke latent visual thoughts and how to use them for quality-sensitive evidence reconstruction. As illustrated in Stage I of Fig. 2, to build a quality-aware reasoning substrate, we particularly use an ROI-based training strategy, where we enforce the routing of visual evidence relevant to the query through the latent tokens. In practice, we implement this constraint by

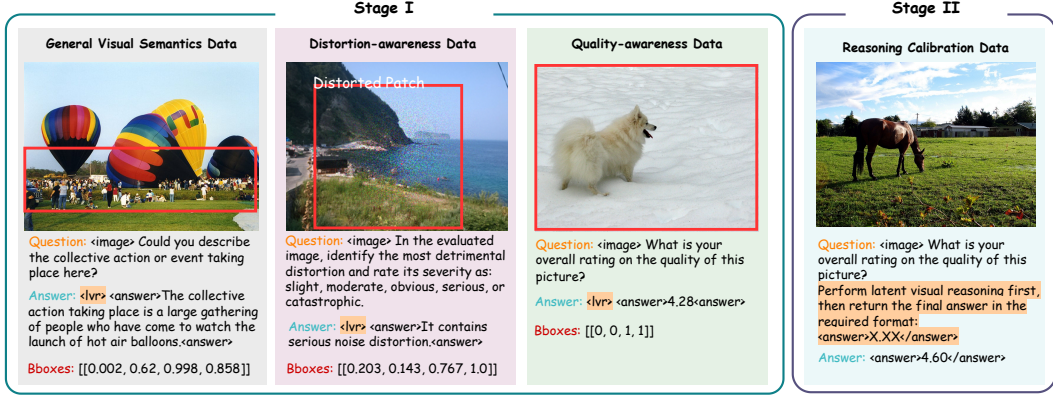


Figure 3: **Example training data for Q-Tacit.** The left part shows the mixture for constructing the latent space in Stage I. The Bboxes field specifies the ROI to supervise latent reconstruction. `<lvr>` functions as a placeholder to indicate where the latent segment should be inserted, which will expand to a series of latent span `<|lvr_start|> <|lvr|>...<|lvr|><|lvr_end|>` in practice. The right part is quality-aligned calibration for latent quality reasoning in Stage II.

providing the model with answer-relevant image regions specified by bounding boxes. Concretely, each input query is paired with an answer-relevant image region, which is obtained via cost-free spatial synthesis.

Given an ROI of the input image, we first convert it into patch-grid coordinates to obtain an index set  $\mathcal{I} = \{i_1, \dots, i_{T_v}\}$ , where  $T_v = |\mathcal{I}|$ , and  $|\mathcal{I}|$  denotes the length of ROI visual index. The corresponding ROI visual tokens are selected from the full set of image tokens as  $V_{\text{ROI}} = \{v_i \mid i \in \mathcal{I}\}$ .

As shown by the example in Fig. 3, each answer begins with the `<lvr>` tag, which will expand into a latent segment representing the reasoning process, i.e., `<|lvr_start|> <|lvr|>_i ... <|lvr|>_T <|lvr_end|>`, where `<|lvr|>` functions as a placeholder for the latent slot. The extracted  $V_{\text{ROI}}$  is then mapped to the reasoning segment. In Stage I, we typically set the number of latent slots to match the ROI token count (i.e.,  $T = T_v$ ) to provide dense token-level supervision, and align each  $i \in \mathcal{I}$  to the corresponding latent step `<|lvr|>_i` via the token index projector  $\phi(\cdot)$ . We then impose a reconstruction objective by treating  $V_{\text{ROI}}$  as targets and training the aligned latent slots to reconstruct the ROI visual tokens indicated in Fig. 2, optimized by Eq. (2). This joint supervision injects quality-relevant ROI evidence into the latent segment and facilitates a quality-aware latent space for subsequent reasoning and calibration.

### 3.2.2 Stage II: Quality-aligned Calibration via Latent GRPO

As shown in Fig. 2, while Stage I is trained with supervised objectives under teacher-forcing, Stage II calibrates the end-to-end scoring behavior via Reinforcement Learning (RL) on the reasoning calibration data (Fig. 3, right), aligning the model with human-rated quality scores. In Stage II, we use a fixed latent-step budget  $T$  because ROI token counts are unavailable for real IQA data. This fixed budget stabilizes policy optimization by keeping trajectory length and compute consistent, and making KL regularization easier to control.

**Reward design.** Since the final output is evaluated solely by its scalar score, rewards are computed from (i) format validity and (ii) the parsed score  $\hat{s}$  between `<answer>` and `</answer>`.

**1) Format compliance reward  $r_{\text{fmt}}$ .** We use a binary reward to enforce structural validity:  $r_{\text{fmt}} = 1$  if the response contains a valid latent segment bounded by `<|lvr_start|> ... <|lvr_end|>` and a parsable `<answer></answer>` with a numeric value inside; otherwise,  $r_{\text{fmt}} = 0$ . This term prevents the policy from drifting away from the intended hybrid interface during RL.

**2) Dense quality scoring reward  $r_{\text{gauss}}$ .** To avoid sparse supervision, we shape score accuracy with a continuous Gaussian kernel:

$$r_{\text{gauss}} = \begin{cases} \exp\left(-\frac{(\hat{s}-s)^2}{2\sigma^2}\right), & \text{if } |\hat{s} - s| \leq \tau \\ 0, & \text{otherwise,} \end{cases} \quad (5)$$

where  $s$  is the ground-truth quality score,  $\sigma$  controls tolerance, and  $\tau$  truncates overly inaccurate predictions to reduce noisy gradients early in training. This yields smooth, bounded feedback (in  $[0, 1]$ ).

**Total reward and advantage.** We combine these two terms as  $r_{\text{total}} = r_{\text{gauss}} + r_{\text{fmt}}$ , where  $r_{\text{gauss}} \in [0, 1]$  and  $r_{\text{fmt}} \in \{0, 1\}$ . Following GRPO, for each input, we sample  $K$  rollouts, compute group-relative advantages by centering rewards within the group, and optimize the objective in Eq. (4).

### 3.2.3 Inference and output format.

At inference, we implement a two-mode decoding procedure. Once `<|1vr_start|>` is produced, the model enters the latent reasoning mode and iteratively computes a sequence of latent hidden states  $\{h_t\}_{t=1}^T$ , and then exits the latent segment by generating `<|1vr_end|>`. We enforce a fixed latent-step budget  $T$ . If `<|1vr_end|>` is not generated before reaching  $T$ , we append it to close the segment to ensure a consistent reasoning length. The final visible output is a scalar score enclosed by `<answer>` and `</answer>`, as shown in Fig. 2.

## 3.3 Data Construction

Data composition diversifies for the two stages, which is detailed in Fig. 3. In **Stage I**, we first incorporate queries on high-level visual recognition to build a general visual semantic substrate for the latent reasoning space, and further include IQA-specific queries to instill a quality-centric prior. Specifically, for distortion awareness, each input consists of a prompt and an image containing a distorted patch via a randomly generated ROI mask. There are five distortion types, including “noise”, “compression”, “blur”, “photometric”, and “null” (no distortion). Each distortion has five severity levels, including “slight”, “moderate”, “obvious”, “serious”, and “catastrophic”. We mix diversified prompts to reduce rigid model responses. For quality-awareness, human-annotated quality scores encourage quality rating prior into the reasoning space. As such, these multi-purpose data sources are complementary, where the high-level vision part stabilizes generic latent thinking behaviors, whereas the IQA-specific queries anchor the latent space to the target perceptual quality dimension. In **Stage II**, we employ queries on image quality ratings to calibrate the model’s reasoning trajectories towards human perception via latent GRPO. More detailed data usage is elaborated in Section 4.1.

## 4 Experiments

### 4.1 Implementation Details

We adopt Qwen2.5-VL-7B-Instruct [1] as the backbone model. The visual encoder and multimodal projector are kept frozen, with only LLM parameters updated throughout training. All training runs on 16×NVIDIA GH200 120GB GPUs [33] with a total batch-size of 128.

For **Stage I**, we randomly sampled 13K data from the Visual CoT dataset [42] for general visual semantics. We also sampled 40K images from KADIS-700K [28] for distortion awareness, and employed the training split of KonIQ-10K [18] for quality awareness, containing 7K images following [63]. The adaptive multimodal data-packing strategy [9] was employed to support dynamic batching. The learning rate is  $1 \times 10^{-5}$ , and  $\lambda_{\text{ivr}}$  is set to 0.1. It takes about 2 hours to complete 4 epochs for convergence. **Stage II** performs quality-aligned quality calibration on the training split of KonIQ-10K. The group size for rollouts is set to 8. The weight of the KL divergence penalty  $\beta$  is  $1 \times 10^{-3}$ , the budget  $T$  is set to 8,  $\sigma = 0.5$ , and  $\tau = 1$ . Besides, the AdamW optimizer [31] is employed with an initial learning rate of  $1 \times 10^{-6}$ . The model is trained for 10 epochs for this phase, taking approximately 25 hours.

Table 1: **PLCC / SRCC results of NR-IQA models trained on KonIQ-10K**. Exceptions marked with <sup>†</sup> use a multi-task training set in [25] for GRPO calibration. Top two results are highlighted in **bold** and underlined, respectively.

Methods	KonIQ-10K	SPAQ	KADID	PIPAL	LIVEW	AGIQA	CSIQ	AVG.
<b>Handcrafted</b>								
NIQE [35]	0.533	0.679	0.468	0.195	0.493	0.560	0.718	0.521
(SPL 2012)	/0.530	/0.664	/0.405	/0.161	/0.449	/0.533	/0.628	/0.481
BRISQUE [34]	0.225	0.490	0.429	0.267	0.361	0.541	0.740	0.436
(TIP 2012)	/0.226	/0.406	/0.356	/0.232	/0.313	/0.497	/0.556	/0.369
<b>Non-VLM Deep-learning</b>								
NIMA [46]	0.896	0.838	0.532	0.390	0.814	0.715	0.695	0.697
(TIP 2018)	/0.859	/0.856	/0.535	/0.399	/0.771	/0.654	/0.649	/0.675
MUSIQ [20]	0.924	0.868	0.575	0.431	0.789	0.722	0.771	0.726
(ICCV 2021)	/0.929	/0.863	/0.556	/0.431	/0.830	/0.630	/0.710	/0.707
CLIP-IQA+ [50]	0.909	0.866	0.653	0.427	0.832	0.736	0.772	0.742
(AAAI 2023)	/0.895	/0.864	/0.654	/0.419	/0.805	/0.685	/0.719	/0.720
ManIQA [60]	0.849	0.768	0.499	0.457	0.849	0.723	0.623	0.681
(CVPR 2022)	/0.834	/0.758	/0.465	/0.452	/0.832	/0.636	/0.627	/0.658
<b>VLM-based</b>								
Compare2Score [75]	0.923	0.867	0.500	0.354	0.786	0.777	0.735	0.706
(NeurIPS 2024)	/0.910	/0.860	/0.453	/0.342	/0.772	/0.671	/0.705	/0.673
Qwen-2.5-VL-7B [1]	0.889	0.874	0.668	0.473	0.734	0.813	0.674	0.732
(Arxiv 2025)	/0.866	/0.875	/0.663	/0.442	/0.728	/0.739	/0.650	/0.709
Q-Align [56]	<u>0.941</u>	0.886	0.674	0.403	0.853	0.772	0.671	0.705
(ICML 2024)	<u>0.940</u>	/0.887	/0.684	/0.419	/0.860	/0.735	/0.737	/0.752
DeQA-Score [63]	<b>0.953</b>	0.895	0.694	0.472	<b>0.892</b>	0.809	0.787	0.786
(CVPR 2025)	<b>0.941</b>	/0.896	/0.687	/0.478	<b>0.879</b>	/0.729	/0.744	/0.765
VisualQuality-R1 [58]	0.924	0.894	0.701	0.469	0.873	0.822	0.743	0.775
(NeurIPS 2025)	/0.915	/0.895	/0.694	/0.446	/0.841	<b>0.773</b>	/0.689	/0.750
Q-Insight [25]	0.918	0.903	0.702	0.458	0.870	0.816	0.685	0.765
(NeurIPS 2025)	/0.895	/0.899	/0.702	/0.435	/0.839	/0.766	/0.640	/0.739
Q-Insight <sup>†</sup> [25]	0.933	0.907	0.742	0.486	<b>0.893</b>	0.811	0.870	0.806
(NeurIPS 2025)	/0.916	/0.905	/0.736	/0.474	/0.865	/0.764	/0.824	/0.783
<b>Q-Tacit</b>	0.923	<u>0.911</u>	<u>0.754</u>	<u>0.488</u>	0.875	<u>0.823</u>	<u>0.879</u>	<u>0.808</u>
<b>(Ours)</b>	/0.914	<u>0.923</u>	<u>0.749</u>	<u>0.493</u>	/0.832	<u>0.765</u>	<u>0.842</u>	<u>0.788</u>
<b>Q-Tacit<sup>†</sup></b>	0.925	<b>0.913</b>	<b>0.766</b>	<b>0.511</b>	0.890	<b>0.828</b>	<b>0.885</b>	<b>0.817</b>
<b>(Ours)</b>	/0.914	<b>0.924</b>	<b>0.760</b>	<b>0.489</b>	<u>0.866</u>	<u>0.769</u>	<b>0.850</b>	<b>0.796</b>

## 4.2 Competing Models and Evaluation Datasets

We report IQA performance across four types of datasets: (1) in-the-wild: KonIQ-10K [18], SPAQ [11], and LIVE-Wild [12]; (2) synthetic distortions: KADID [27] and CSIQ [21]; (3) model-processed distortions: PIPAL [14]; and (4) AI-generated: AGIQA [23]. MOSs of these datasets are normalized to the range of [1,5], with the variances normalized accordingly. We compare **Q-Tacit** with handcrafted methods NIQE [35] and BRISQUE [34]; deep-learning methods including NIMA [46], MUSIQ [20], CLIP-IQA+ [50], and ManIQA [60]; and recent VLM-based methods, including Compare2Score [75], Q-Align [56], DeQA-Score [63], Q-Insight [25], VisualQuality-R1 [58] and supervised fine-tuned Qwen-2.5-VL-7B [1]. These VLM-based methods contain approximately 7B parameters. For a fair comparison, all compared models are trained on KonIQ-10K [18], unless explicitly stated otherwise. We adopt PLCC and SRCC to measure performance following [60, 56].

## 4.3 Main Results

We compare the quality prediction performance of **Q-Tacit** with other IQA methods in Table 1 with the following key observations. Firstly, VLM-based methods outperform traditional and discriminating deep-learning-based methods, with Qwen-2.5-VL exhibiting strong zero-shot quality scoring ability, indicating the competence of VLMs. Secondly, reasoning-induced methods such as Q-Insight, VisualQuality-R1, and Q-Tacit, offer better cross-dataset generalization compared to pure SFT-based methods such as Q-Align and DeQA-Score. Thirdly, Q-Tacit achieves the best performance on

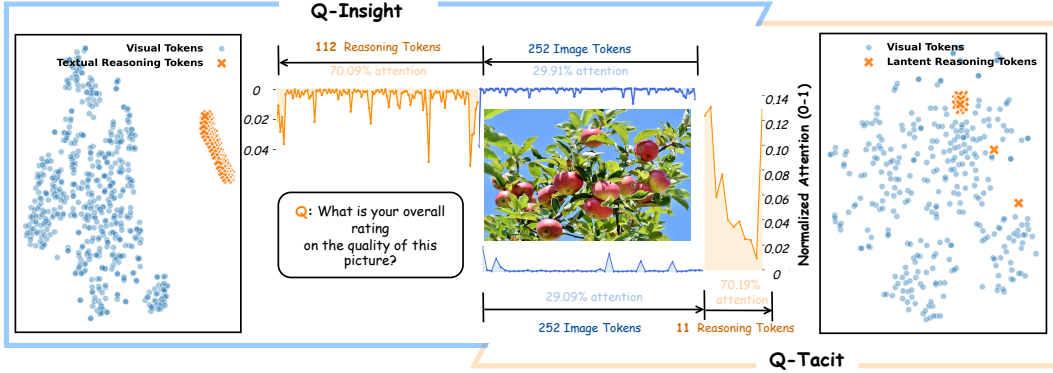


Figure 4: **Token-space coupling and attention weight distribution during quality scoring: Q-Insight vs. Q-Tacit.** Left/Right: t-SNE visualization of visual and reasoning tokens for Q-Insight/Q-Tacit. Middle: normalized attention weights over the image and reasoning tokens after the quality score is generated. Q-Tacit obtained similar attention allocated to reasoning with only 11 tokens (vs. 112 for Q-Insight).

average, indicating that reasoning in latent space aligns better with human perception of quality than text-centric quality reasoning. Moreover, Q-Tacit enables scalable calibration of reasoning trajectories via Stage II’s training. We exploit this and train Q-Tacit<sup>†</sup> on the training data of Q-Insight<sup>†</sup> [25], which contains additional image distortion perception data. As shown in the last two lines of Table 1, Q-Tacit<sup>†</sup> yields consistent gains across all seven datasets and achieves state-of-the-art performance among all compared models. This reflects the effectiveness of latent-space reasoning supervision for learning transferable quality representations. Overall, these provide empirical support for the precondition that a compact latent space can operate more directly on perceptual evidence, thereby improving generalization ability.

To further investigate the mechanism underlying Q-Tacit’s effectiveness, we compare the attention patterns of Q-Insight and Q-Tacit during scoring. Specifically, we normalize the image and reasoning tokens after the quality score is generated and visualize them. As illustrated in Fig. 4, quality score generation predominantly attends to reasoning tokens for both methods. Q-Tacit assigns a larger fraction of attention to its reasoning tokens than the text-centric Q-Insight, with far fewer reasoning tokens ( $\approx 10\%$ ). Besides, t-SNE [49] visualizations show that Q-Tacit’s reasoning tokens are more interleaved with visual tokens, suggesting tighter coupling to visual embeddings. This indicates that the latent space compactly encodes quality-relevant visual evidence, further supporting latent continuous space as a favorable alternative to purely language-centric reasoning for IQA.

Moreover, we probe whether the proposed Q-Tacit can reason with concrete visual quality evidence and respond to subtle local degradations. As shown in Fig. 5, we manually insert a distorted patch into otherwise unchanged images, and compare the predicted quality of Q-Tacit with other two reasoning-induced methods, Q-Insight [25] and VisualQuality-R1 [58] using their original reasoning prompt templates. Q-Tacit consistently lowers its predicted scores in response to the local distortion, whereas Q-Insight and VisualQuality-R1 are markedly less sensitive. This indicates that Q-Tacit’s latent reasoning is more visual-aware than text-centric reasoning.

#### 4.4 Ablation Studies

**Study1: Effect of latent reasoning.** We first verify that the gain of Q-Tacit stems from the proposed latent-space reasoning mode, rather than from additional training beyond RL or from RL alone. We compare (i) Stage I-only, and (ii) Stage I+Stage II without the LVR mode. As shown in Table 2, the non-LVR variant matches in-domain performance on KonIQ-10K, but exhibits noticeably weaker OOD generalization. In contrast, enabling latent reasoning consistently improves cross-dataset robustness. These clearly indicate that the observed gains are primarily driven by latent-space reasoning, whereas neither additional training nor RL alone can account for the full improvements.



Figure 5: **Sensitivity to localized distortions.** We compare Q-Insight, VisualQuality-R1, and Q-Tacit by reporting predicted quality scores for each image (w/o distorted patch, top) and its counterpart with a localized corruption (w/ distorted patch, bottom). Blur, noise, and compression are injected within the red box (left to right). Q-Tacit consistently lowers its predicted scores in response to the local distortion.

Table 2: **Ablation on the effect of latent reasoning pipeline (PLCC/SRCC).** We compare Q-Tacit with two variants: *Stage I-only* and *Stage I+II w/o LVR*. Top two results are highlighted in **bold** and underlined, respectively.

Training Strategy	KonIQ-10K	SPAQ	KADID	PIPAL	LIVEW	AGIQA	CSIQ
Stage I only	0.901/0.899	<u>0.904/0.901</u>	0.733/0.731	0.473/0.467	0.853/0.811	<u>0.812/0.737</u>	0.839/0.802
Stage I+II w/o LVR	<u>0.920/0.912</u>	0.901/0.898	<u>0.736/0.735</u>	<u>0.476/0.475</u>	<u>0.871/0.834</u>	0.809/0.759	<u>0.867/0.825</u>
Q-Tacit (Ours)	<b>0.923/0.914</b>	<b>0.911/0.923</b>	<b>0.754/0.749</b>	<b>0.488/0.493</b>	<b>0.875/0.832</b>	<b>0.823/0.765</b>	<b>0.879/0.842</b>

Table 3: **Ablation on the latent space composition (PLCC/SRCC).** We vary the Stage I training data on three subsets ( $\checkmark$  indicates included data), while keeping Stage II identical across rows. Top two results are highlighted in **bold** and underlined, respectively.

General Vision	Quality awareness	Distortion awareness	KonIQ-10K	SPAQ	KADID	PIPAL	LIVEW	AGIQA	CSIQ
$\checkmark$			0.901/0.889	0.895/0.892	0.701/0.699	0.453/0.437	0.869/ <u>0.832</u>	0.820/ <b>0.769</b>	0.688/0.655
$\checkmark$		$\checkmark$	<b>0.920/0.915</b>	<b>0.909/0.918</b>	<b>0.753/0.749</b>	<b>0.482/0.491</b>	<b>0.875/0.835</b>	<b>0.825/0.761</b>	<b>0.875/0.838</b>
$\checkmark$	$\checkmark$		0.915/0.899	0.903/0.901	0.710/ <u>0.709</u>	0.461/0.450	<u>0.870/0.835</u>	0.818/ <u>0.765</u>	0.732/0.679
$\checkmark$	$\checkmark$	$\checkmark$	<b>0.923/0.914</b>	<b>0.911/0.923</b>	<b>0.754/0.749</b>	<b>0.488/0.493</b>	<b>0.875/0.832</b>	<b>0.823/0.765</b>	<b>0.879/0.842</b>

**Study2: Effect of latent space composition.** Table 3 shows how Stage I forms a usable latent visual reasoning space under three data mixtures: (i) general vision, (ii) general vision + distortion awareness, and (iii) general vision + quality awareness. It can be observed that adding distortion awareness is the most critical to Q-Tacit, since it grounds the general visual latent space to specific quality evidence. Meanwhile, excluding quality awareness introduces a subtle performance drop, but it can slow the subsequent Stage II training in practice. Overall, the full mixture performs best, suggesting a complementary role of the components, where high-level data stabilizes generic latent reasoning, while IQA-specific perception and scoring anchor the latent space to perceptual quality, thus improving generalization.

**Study3: Effect of reward function in latent GRPO.** To evaluate the contribution of the proposed reward function described in Sec. 3.2.2, we compare it with two alternatives: Q-Insight [25] and R2RL [58]. We also assess the sensitivity to the threshold  $\tau$  in  $r_{gauss}$  (Eq. (5)). As reported in Table 3, our proposed reward function yields higher performance compared to the other two, suggesting that our reward can better guide reasoning calibration. Besides, Q-Tacit achieves relatively stable performance across different threshold values  $\tau$ , but it should not be too loose or too tight.

**Study4: Effect of latent reasoning budget  $T$ .** We vary the latent reasoning budget  $T$  aside from the default  $T = 8$ , which controls the number of latent update steps. Table 5 shows that either

Table 4: **Ablation on reward design (PLCC/SRCC)**. Q-Insight and R2RL are two different reward design, and  $\tau$  is the threshold in our dense quality scoring reward. Top two results are highlighted in **bold** and underlined, respectively.

Reward	KonIQ-10K	SPAQ	KADID	PIPAL	LIVEW	AGIQA	CSIQ
Q-Insight [25]	<b>0.928/0.908</b>	0.901/0.903	0.743/0.735	0.481/0.479	0.855/0.812	0.812/0.758	0.856/ <u>0.834</u>
R2RL [58]	0.922/0.907	0.905/ <u>0.913</u>	<b>0.756/0.745</b>	<u>0.485/0.481</u>	<b>0.859/0.827</b>	0.815/ <u>0.761</u>	0.863/0.827
$\tau = 0.35$	<u>0.924/0.914</u>	<u>0.908/0.913</u>	0.752/ <b>0.749</b>	0.479/0.475	<u>0.859/0.815</u>	<u>0.820/0.760</u>	0.864/0.823
$\tau = 2$	0.921/ <u>0.908</u>	0.901/0.905	0.753/ <u>0.747</u>	0.483/ <u>0.487</u>	0.855/0.819	0.814/0.750	<u>0.870/0.833</u>
$\tau = 1$ (Ours)	0.923/ <b>0.914</b>	<b>0.911/0.923</b>	<u>0.754/0.749</u>	<b>0.488/0.493</b>	<b>0.875/0.832</b>	<b>0.823/0.765</b>	<b>0.879/0.842</b>

Table 5: **Ablation on latent reasoning budget  $T$  (PLCC/SRCC)**. We vary the latent-segment length  $T \in \{4, 16\}$  and compare with the default setting  $T = 8$ . Top two results are highlighted in **bold** and underlined, respectively.

Budget	KonIQ-10K	SPAQ	KADID	PIPAL	LIVEW	AGIQA	CSIQ
$T = 4$	<u>0.920/0.913</u>	0.910/ <b>0.924</b>	0.745/0.740	0.481/0.489	<u>0.871/0.829</u>	0.812/0.749	<u>0.864/0.826</u>
$T = 16$	0.919/0.910	<b>0.912/0.922</b>	<b>0.755/0.751</b>	<u>0.487/0.492</u>	0.870/0.828	<b>0.824/0.766</b>	<b>0.879/0.843</b>
$T = 8$ (Ours)	<b>0.923/0.914</b>	<u>0.911/0.923</u>	<u>0.754/0.749</u>	<b>0.488/0.493</b>	<b>0.875/0.832</b>	<u>0.823/0.765</u>	<b>0.879/0.842</b>

reducing  $T$  to 4 or increasing it to 16 has only a marginal effect, offering an advantageous trade-off between computational complexity and performance.

## 5 Conclusions

In this paper, we introduce **Q-Tacit**, a reasoning-induced NR-IQA framework that enhances the reasoning processes for image quality assessment in a continuous latent visual space. Unlike prior VLM-based IQA approaches that mainly leverage long textual rationales, **Q-Tacit** frames quality assessment as latent evidence reconstruction and aggregation, enabling compact, visually grounded reasoning with a strict score-only output. Our two-stage recipe injects structural visual quality priors into the latent space via multi-task SFT and further calibrates latent reasoning trajectories with latent GRPO, improving robustness under diverse distortion regimes. Extensive experiments across authentic, synthetic, model-processed, and AI-generated benchmarks demonstrate strong cross-dataset generalization and competitive in-domain performance, while ablations confirm the contribution of latent mode control, data composition, reward shaping, and reasoning budget. We believe **Q-Tacit** provides a useful perspective for future IQA research on latent-space reasoning, and may be extended to other perceptual rating tasks or combined with agentic visual tools for more controllable quality analysis.

## Acknowledgment

The authors appreciate the funding from the University of Bristol, and the UKRI MyWorld Strength in Places Programme (SIPF00006/1). We also acknowledge the use of resources provided by the Isambard-AI National AI Research Resource (AIRR). Isambard-AI is operated by the University of Bristol and is funded by the UK Government’s Department for Science, Innovation and Technology (DSIT) via UK Research and Innovation; and the Science and Technology Facilities Council [ST/AIRR/I-A-I/1023].

## References

- [1] Shuai Bai, Keqin Chen, Xuejing Liu, Jialin Wang, Wenbin Ge, Sibao Song, Kai Dang, Peng Wang, Shijie Wang, Jun Tang, Humen Zhong, Yuanzhi Zhu, Mingkun Yang, Zhaohai Li, Jianqiang Wan, Pengfei Wang, Wei Ding, Zheren Fu, Yiheng Xu, Jiabo Ye, Xi Zhang, Tianbao Xie, Zesen Cheng, Hang Zhang, Zhibo Yang, Haiyang Xu, Junyang Lin, et al. Qwen2.5-VL Technical Report. *arXiv preprint arXiv:2502.13923*, 2025.

- [2] Sebastian Bosse, Dominique Maniry, Klaus-Robert Müller, Thomas Wiegand, and Wojciech Samek. Deep neural networks for no-reference and full-reference image quality assessment. *IEEE Transactions on Image Processing (TIP)*, 27(1):206–219, 2017.
- [3] Rui Cai, Bangzheng Li, Xiaofei Wen, Muhao Chen, and Zhe Zhao. Diagnosing and Mitigating Modality Interference in Multimodal Large Language Models. *arXiv preprint arXiv:2505.19616*, 2025.
- [4] Zhuoxuan Cai, Jian Zhang, Xinbin Yuan, Pengtao Jiang, Wenxiang Chen, Bowen Tang, Lujian Yao, Qiyuan Wang, Jinwen Chen, and Bo Li. Q-Ponder: A Unified Training Pipeline for Reasoning-based Visual Quality Assessment. *arXiv preprint arXiv:2506.05384*, 2025.
- [5] Baoliang Chen, Haoliang Li, Hongfei Fan, and Shiqi Wang. No-Reference Screen Content Image Quality Assessment With Unsupervised Domain Adaptation. *IEEE Transactions on Image Processing (TIP)*, 30:5463–5476, 2021.
- [6] Chao Chen, Zhixin Ma, Yongqi Li, Yupeng Hu, Yinwei Wei, Wenjie Li, and Liqiang Nie. Reasoning in the dark: Interleaved vision-text reasoning in latent space. *arXiv preprint arXiv:2510.12603*, 2025.
- [7] Du Chen, Tianhe Wu, Kede Ma, and Lei Zhang. Toward Generalized Image Quality Assessment: Relaxing the Perfect Reference Quality Assumption. In *Proceedings of the IEEE/CVF Conference on Computer Vision and Pattern Recognition (CVPR)*, pages 12742–12752, 2025.
- [8] Harold Haodong Chen, Xinxiang Yin, Wen-Jie Shu, Hongfei Zhang, Zixin Zhang, Chenfei Liao, Litao Guo, Qifeng Chen, and Ying-Cong Chen. Show, Don’t Tell: Morphing Latent Reasoning into Image Generation. *arXiv preprint arXiv:2602.02227*, 2026.
- [9] Zhe Chen, Weiyun Wang, Yue Cao, Yangzhou Liu, Zhangwei Gao, Erfei Cui, Jinguo Zhu, Shenglong Ye, Hao Tian, Zhaoyang Liu, et al. Expanding Performance Boundaries of Open-Source Multimodal Models with Model, Data, and Test-Time Scaling. *arXiv preprint arXiv:2412.05271*, 2024.
- [10] Jeffrey Cheng and Benjamin Van Durme. Compressed Chain of Thought: Efficient Reasoning Through Dense Representations. *arXiv preprint arXiv:2412.13171*, 2024.
- [11] Yuming Fang, Hanwei Zhu, Yan Zeng, Kede Ma, and Zhou Wang. Perceptual Quality Assessment of Smartphone Photography. In *Proceedings of the IEEE/CVF Conference on Computer Vision and Pattern Recognition (CVPR)*, pages 3677–3686, 2020.
- [12] Deepti Ghadiyaram and Alan C Bovik. LIVE In the Wild Image Quality Challenge Database. *Online*, 2015.
- [13] Sachin Goyal, Ziwei Ji, Ankit Singh Rawat, Aditya Krishna Menon, Sanjiv Kumar, and Vaishnavh Nagarajan. Think before you speak: Training Language Models With Pause Tokens. *arXiv preprint arXiv:2310.02226*, 2023.
- [14] Jinjin GU, Haoming Cai, Haoyu Chen, Xiaoxing Ye, Ren Jimmy S, and Chao Dong. PIPAL: a Large-Scale Image Quality Assessment Dataset for Perceptual Image Restoration. In *Proceedings of the European Conference on Computer Vision (ECCV)*, pages 633–651. Springer, 2020.
- [15] Daya Guo, Dejian Yang, Haowei Zhang, Junxiao Song, Peiyi Wang, Qihao Zhu, Runxin Xu, Ruoyu Zhang, Shirong Ma, Xiao Bi, et al. Deepseek-r1: Incentivizing reasoning capability in llms via reinforcement learning. *arXiv preprint arXiv:2501.12948*, 2025.
- [16] Shibo Hao, Sainbayar Sukhbaatar, DiJia Su, Xian Li, Zhiting Hu, Jason Weston, and Yuandong Tian. Training Large Language Models to Reason in a Continuous Latent Space. *arXiv preprint arXiv:2412.06769*, 2024.
- [17] David Holz. Midjourney. <https://www.midjourney.com/>, 2023.
- [18] Vlad Hosu, Hanhe Lin, Tamas Sziranyi, and Dietmar Saupe. KonIQ-10k: An ecologically valid database for deep learning of blind image quality assessment. *IEEE Transactions on Image Processing (TIP)*, 29:4041–4056, 2020.
- [19] Wenxuan Huang, Bohan Jia, Zijie Zhai, Shaosheng Cao, Zheyu Ye, Fei Zhao, Zhe Xu, Yao Hu, and Shaohui Lin. Vision-r1: Incentivizing reasoning capability in multimodal large language models. *arXiv preprint arXiv:2503.06749*, 2025.

- [20] Junjie Ke, Qifei Wang, Yilin Wang, Peyman Milanfar, and Feng Yang. MUSIQ: Multi-Scale Image Quality Transformer. In *Proceedings of the IEEE/CVF International Conference on Computer Vision (ICCV)*, pages 5148–5157, 2021.
- [21] Eric C Larson and Damon M Chandler. Most apparent distortion: full-reference image quality assessment and the role of strategy. *Journal of Electronic Imaging*, 19(1):011006–011006, 2010.
- [22] Bangzheng Li, Ximeng Sun, Jiang Liu, Ze Wang, Jialian Wu, Xiaodong Yu, Hao Chen, Emad Barsoum, Muhao Chen, and Zicheng Liu. Latent visual reasoning. *arXiv preprint arXiv:2509.24251*, 2025.
- [23] Chunyi Li, Zicheng Zhang, Haoning Wu, Wei Sun, Xiongkuo Min, Xiaohong Liu, Guangtao Zhai, and Weisi Lin. AGIQA-3K: An Open Database for AI-Generated Image Quality Assessment. *IEEE Transactions on Circuits and Systems for Video Technology (TCSVT)*, 34(8):6833–6846, 2023.
- [24] Kelvin Li, Chuyi Shang, Leonid Karlinsky, Rogerio Feris, Trevor Darrell, and Roei Herzig. Latent implicit visual reasoning. *arXiv preprint arXiv:2512.21218*, 2025.
- [25] Weiqi Li, Xuanyu Zhang, Shijie Zhao, Yabin Zhang, Junlin Li, Li Zhang, and Jian Zhang. Q-insight: Understanding image quality via visual reinforcement learning. *arXiv preprint arXiv:2503.22679*, 2025.
- [26] Guoqiang Liang, Jianyi Wang, Zhonghua Wu, and Shangchen Zhou. Zoom-IQA: Image quality assessment with reliable region-aware reasoning. *arXiv preprint arXiv:2601.02918*, 2026.
- [27] Hanhe Lin, Vlad Hosu, and Dietmar Saupe. KADID-10k: A Large-scale Artificially Distorted IQA Database. In *Proceedings of International Conference on Quality of Multimedia Experience (QoMEX)*, pages 1–3. IEEE, 2019.
- [28] Hanhe Lin, Vlad Hosu, and Dietmar Saupe. DeepFL-IQA: Weak Supervision for Deep IQA Feature Learning. *arXiv preprint arXiv:2001.08113*, 2020.
- [29] Haotian Liu, Chunyuan Li, Qingyang Wu, and Yong Jae Lee. Visual Instruction Tuning. *Proceedings of the Advances in Neural Information Processing Systems (NeurIPS)*, 36:34892–34916, 2023.
- [30] Ziyu Liu, Zeyi Sun, Yuhang Zang, Xiaoyi Dong, Yuhang Cao, Haodong Duan, Dahua Lin, and Jiaqi Wang. Visual-RFT: Visual Reinforcement Fine-Tuning. *arXiv preprint arXiv:2503.01785*, 2025.
- [31] Ilya Loshchilov and Frank Hutter. Decoupled Weight Decay Regularization. In *International Conference on Learning Representations (ICLR)*, 2019.
- [32] Jizheng Ma, Xiaofei Zhou, Yanlong Song, and Han Yan. Cocova: Chain of continuous vision-language thought for latent space reasoning. *arXiv e-prints*, pages arXiv–2511, 2025.
- [33] Simon McIntosh-Smith, Sadaf Alam, and Christopher Woods. Isambard-AI: a leadership-class supercomputer optimised specifically for artificial intelligence. In *Proceedings of the Cray User Group*, pages 44–54. 2024.
- [34] Anish Mittal, Anush Krishna Moorthy, and Alan C. Bovik. No-Reference Image Quality Assessment in the Spatial Domain. *IEEE Transactions on Image Processing (TIP)*, 21(12):4695–4708, 2012.
- [35] Anish Mittal, Rajiv Soundararajan, and Alan C. Bovik. Making a “Completely Blind” Image Quality Analyzer. *IEEE Signal Processing Letters*, 20(3):209–212, 2013.
- [36] Hans P. Moravec. *Mind Children: The Future of Robot and Human Intelligence*. Harvard University Press, Cambridge, MA, 1988.
- [37] Alexander Quinn Nichol, Prafulla Dhariwal, Aditya Ramesh, Pranav Shyam, Pamela Mishkin, Bob McGrew, Ilya Sutskever, and Mark Chen. GLIDE: Towards photorealistic image generation and editing with text-guided diffusion models. In *International Conference on Machine Learning*, pages 16784–16804. PMLR, 2022.
- [38] Yiming Qin, Bomini Wei, Jiaxin Ge, Konstantinos Kallidromitis, Stephanie Fu, Trevor Darrell, and XuDong Wang. Chain-of-visual-thought: Teaching VLMs to see and think better with continuous visual tokens. *arXiv preprint arXiv:2511.19418*, 2025.

- [39] Aditya Ramesh, Prafulla Dhariwal, Alex Nichol, Casey Chu, and Mark Chen. Hierarchical text-conditional image generation with clip latents. *arXiv preprint arXiv:2204.06125*, 2022.
- [40] Robin Rombach, Andreas Blattmann, Dominik Lorenz, Patrick Esser, and Björn Ommer. High-resolution image synthesis with latent diffusion models. In *Proceedings of the IEEE/CVF Conference on Computer Vision and Pattern Recognition*, pages 10684–10695, 2022.
- [41] Robin Rombach, Andreas Blattmann, and Björn Ommer. Text-guided synthesis of artistic images with retrieval-augmented diffusion models. *arXiv preprint arXiv:2207.13038*, 2022.
- [42] Hao Shao, Shengju Qian, Han Xiao, Guanglu Song, Zhuofan Zong, Letian Wang, Yu Liu, and Hongsheng Li. Visual cot: Unleashing chain-of-thought reasoning in multi-modal language models. *arXiv preprint arXiv:2403.16999*, 2, 2024.
- [43] Zhihong Shao, Peiyi Wang, Qihao Zhu, Runxin Xu, Junxiao Song, Xiao Bi, Haowei Zhang, Mingchuan Zhang, YK Li, Yang Wu, et al. Deepseekmath: Pushing the limits of mathematical reasoning in open language models. *arXiv preprint arXiv:2402.03300*, 2024.
- [44] Zhenyi Shen, Hanqi Yan, Linhai Zhang, Zhanghao Hu, Yali Du, and Yulan He. CODI: Compressing Chain-of-Thought into Continuous Space via Self-Distillation. In *Proceedings of the 2025 Conference on Empirical Methods in Natural Language Processing*, pages 677–693, 2025.
- [45] Zhiqing Sun, Sheng Shen, Shengcao Cao, Haotian Liu, Chunyuan Li, Yikang Shen, Chuang Gan, Liang-Yan Gui, Yu-Xiong Wang, Yiming Yang, et al. Aligning Large Multimodal Models with Factually Augmented RLHF. *arXiv preprint arXiv:2309.14525*, 2023.
- [46] Hossein Talebi and Peyman Milanfar. NIMA: Neural Image Assessment. *IEEE Transactions on Image Processing (TIP)*, 27:3998–4011, 2018.
- [47] Bart Thomee, David A Shamma, Gerald Friedland, Benjamin Elizalde, Karl Ni, Douglas Poland, Damian Borth, and Li-Jia Li. YFCC100M: The new data in multimedia research. *Communications of the ACM*, 59(2):64–73, 2016.
- [48] Yu Tian, Yixuan Li, Baoliang Chen, Hanwei Zhu, Shiqi Wang, and Sam Kwong. AI-generated Image Quality Assessment in Visual Communication. In *Proceedings of the AAAI Conference on Artificial Intelligence*, volume 39-7, pages 7392–7400, 2025.
- [49] Laurens Van der Maaten and Geoffrey Hinton. Visualizing data using t-SNE. *Journal of machine learning research*, 9(11), 2008.
- [50] Jianyi Wang, Kelvin C. K. Chan, and Chen Change Loy. Exploring CLIP for Assessing the Look and Feel of Images. In *Proceedings of the AAAI Conference on Artificial Intelligence (AAAI)*, 2023.
- [51] Qixun Wang, Yang Shi, Yifei Wang, Yuanxing Zhang, Pengfei Wan, Kun Gai, Xianghua Ying, and Yisen Wang. Monet: Reasoning in Latent Visual Space Beyond Images and Language. *arXiv preprint arXiv:2511.21395*, 2025.
- [52] Xuezhi Wang, Jason Wei, Dale Schuurmans, Quoc V. Le, Ed H. Chi, Sharan Narang, Aakanksha Chowdhery, and Denny Zhou. Self-Consistency Improves Chain of Thought Reasoning in Language Models. In *International Conference on Learning Representations (ICLR)*, 2023.
- [53] Zhihua Wang, Haotao Wang, Tianlong Chen, Zhangyang Wang, and Kede Ma. Troubleshooting Blind Image Quality Models in the Wild. In *Proceedings of the IEEE/CVF Conference on Computer Vision and Pattern Recognition (CVPR)*, pages 16256–16265, 2021.
- [54] Jason Wei, Xuezhi Wang, Dale Schuurmans, Maarten Bosma, Brian Ichter, Fei Xia, Ed H. Chi, Quoc V. Le, and Denny Zhou. Chain-of-Thought Prompting Elicits Reasoning in Large Language Models. In *Advances in Neural Information Processing Systems*, volume 35, 2022.
- [55] Haoning Wu, Zicheng Zhang, Erli Zhang, Chaofeng Chen, Liang Liao, Annan Wang, Kaixin Xu, Chunyi Li, Jingwen Hou, Guangtao Zhai, et al. Q-Instruct: Improving Low-level Visual Abilities for Multi-modality Foundation Models. In *Proceedings of the IEEE/CVF Conference on Computer Vision and Pattern Recognition (CVPR)*, pages 25490–25500, 2024.
- [56] Haoning Wu, Zicheng Zhang, Weixia Zhang, Chaofeng Chen, Liang Liao, Chunyi Li, Yixuan Gao, Annan Wang, Erli Zhang, Wenxiu Sun, Qiong Yan, Xiongkuo Min, Guangtao Zhai, and Weisi Lin. Q-Align: Teaching LMMs for Visual Scoring via Discrete Text-Defined Levels. In *Proceedings of the 41st International Conference on Machine Learning*, volume 235 of *Proceedings of Machine Learning Research*, pages 54015–54029. PMLR, 2024.

- [57] Haoning Wu, Hanwei Zhu, Zicheng Zhang, Erli Zhang, Chaofeng Chen, Liang Liao, Chunyi Li, Annan Wang, Wenxiu Sun, Qiong Yan, Xiaohong Liu, Guangtao Zhai, Shiqi Wang, and Weisi Lin. Towards Open-ended Visual Quality Comparison. In *European Conference on Computer Vision (ECCV)*, 2024.
- [58] Tianhe Wu, Jian Zou, Jie Liang, Lei Zhang, and Kede Ma. VisualQuality-R1: Reasoning-Induced Image Quality Assessment via Reinforcement Learning to Rank. *arXiv preprint arXiv:2505.14460*, 2025.
- [59] Tao Xu, Pengchuan Zhang, Qiuyuan Huang, Han Zhang, Zhe Gan, Xiaolei Huang, and Xiaodong He. Attngan: Fine-grained text to image generation with attentional generative adversarial networks. In *Proceedings of the IEEE conference on computer vision and pattern recognition*, pages 1316–1324, 2018.
- [60] Sidi Yang, Tianhe Wu, Shuwei Shi, Shanshan Lao, Yuan Gong, Mingdeng Cao, Jiahao Wang, and Yujiu Yang. MANIQA: Multi-Dimension Attention Network for No-Reference Image Quality Assessment. In *Proceedings of the IEEE/CVF Conference on Computer Vision and Pattern Recognition (CVPR) Workshops*, pages 1191–1200, June 2022.
- [61] Zeyuan Yang, Xueyang Yu, Delin Chen, Maohao Shen, and Chuang Gan. Machine mental imagery: Empower multimodal reasoning with latent visual tokens. *arXiv preprint arXiv:2506.17218*, 2025.
- [62] Shunyu Yao, Dian Yu, Jeffrey Zhao, Izhak Shafran, Thomas L. Griffiths, Yuan Cao, and Karthik Narasimhan. Tree of Thoughts: Deliberate Problem Solving with Large Language Models. In *Advances in Neural Information Processing Systems*, volume 36, 2023.
- [63] Zhiyuan You, Xin Cai, Jinjin Gu, Tianfan Xue, and Chao Dong. Teaching Large Language Models to Regress Accurate Image Quality Scores Using Score Distribution. In *Proceedings of the IEEE/CVF Conference on Computer Vision and Pattern Recognition (CVPR)*, pages 14483–14494, June 2025.
- [64] Zhiyuan You, Jinjin Gu, Zheyuan Li, Xin Cai, Kaiwen Zhu, Chao Dong, and Tianfan Xue. Descriptive Image Quality Assessment in the Wild. *arXiv preprint arXiv:2405.18842*, 2024.
- [65] Zhiyuan You, Zheyuan Li, Jinjin Gu, Zhenfei Yin, Tianfan Xue, and Chao Dong. Depicting Beyond Scores: Advancing Image Quality Assessment through Multi-modal Language Models. In *Proceedings of the European Conference on Computer Vision (ECCV)*, pages 259–276. Springer, 2024.
- [66] Tianyu Yu, Haoye Zhang, Yuan Yao, Yunkai Dang, Da Chen, Xiaoman Lu, Ganqu Cui, Taiwen He, Zhiyuan Liu, Tat-Seng Chua, et al. RLAI-F-V: Aligning MLLMs through Open-Source AI Feedback for Super GPT-4V Trustworthiness. *arXiv preprint arXiv:2405.17220*, 2024.
- [67] Jingyi Zhang, Jiaying Huang, Huanjin Yao, Shunyu Liu, Xikun Zhang, Shijian Lu, and Dacheng Tao. R1-VL: Learning to Reason with Multimodal Large Language Models via Step-wise Group Relative Policy Optimization. *arXiv preprint arXiv:2503.12937*, 2025.
- [68] Qizhe Zhang, Aosong Cheng, Ming Lu, Renrui Zhang, Zhiyong Zhuo, Jiajun Cao, Shaobo Guo, Qi She, and Shanghang Zhang. Beyond Text-Visual Attention: Exploiting Visual Cues for Effective Token Pruning in VLMs. In *Proceedings of the IEEE/CVF International Conference on Computer Vision*, pages 20857–20867, 2025.
- [69] Weixia Zhang, Dingquan Li, Chao Ma, Guangtao Zhai, Xiaokang Yang, and Kede Ma. Continual Learning for Blind Image Quality Assessment. *IEEE Transactions on Pattern Analysis and Machine Intelligence*, 45(3):2864–2878, 2022.
- [70] Xuanyu Zhang, Weiqi Li, Shijie Zhao, Junlin Li, Li Zhang, and Jian Zhang. VQ-Insight: Teaching VLMs for AI-Generated Video Quality Understanding via Progressive Visual Reinforcement Learning. *Proceedings of the AAAI Conference on Artificial Intelligence (AAAI)*, 2026.
- [71] Shijie Zhao, Xuanyu Zhang, Weiqi Li, Junlin Li, Li Zhang, Tianfan Xue, and Jian Zhang. Reasoning as Representation: Rethinking Visual Reinforcement Learning in Image Quality Assessment. *arXiv preprint arXiv:2510.11369*, 2025.
- [72] Zhiyuan Zhao, Bin Wang, Linke Ouyang, Xiaoyi Dong, Jiaqi Wang, and Conghui He. Beyond Multimodal Hallucinations: Enhancing LVLMs through Hallucination-Aware Direct Preference Optimization. In *2025 IEEE International Conference on Multimedia and Expo (ICME)*, pages 1–6. IEEE, 2025.

- [73] Denny Zhou, Nathanael Schärli, Le Hou, Jason Wei, Nathan Scales, Xuezhi Wang, Dale Schuurmans, Claire Cui, Olivier Bousquet, Quoc Le, and Ed H. Chi. Least-to-Most Prompting Enables Complex Reasoning in Large Language Models. In *International Conference on Learning Representations (ICLR)*, 2023.
- [74] Hancheng Zhu, Leida Li, Jinjian Wu, Weisheng Dong, and Guangming Shi. MetaIQA: Deep Meta-learning for No-Reference Image Quality Assessment. In *Proceedings of the IEEE/CVF Conference on Computer Vision and Pattern Recognition (CVPR)*, pages 14143–14152, 2020.
- [75] Hanwei Zhu, Haoning Wu, Yixuan Li, Zicheng Zhang, Baoliang Chen, Lingyu Zhu, Yuming Fang, Guangtao Zhai, Weisi Lin, and Shiqi Wang. Adaptive Image Quality Assessment via Teaching Large Multimodal Model to Compare. *arXiv preprint arXiv:2405.19298*, 2024.

## A More Details on Image Quality Assessment Datasets

The details of the utilized Image Quality Assessment (IQA) datasets are summarized as follows.

- **CSIQ [21]:** The CSIQ database contains 30 reference images and 866 distorted images with 6 distortions of JPEG compression, JPEG2000 compression, Gaussian blur, Gaussian white noise, Gaussian pink noise, and contrast change. The subjective testing method is the single-stimulus absolute category rating. The DMOSs span from 0 to 1.
- **KADID-10k [27]:** The KADID-10k database contains 81 reference images and 10,125 distorted images by adding 25 distortion types with 5 distortion levels, such as blur, color distortions, noise, spatial distortions, etc. The subjective testing method is the double-stimulus continuous quality rating by crowdsourcing. The DMOSs range from 1 to 5.
- **KonIQ-10k [18]:** The KonIQ-10K database consists of 10,073 images with abundant realistic distortions. Those are selected from the YFCC100M database [47]. Single-stimulus absolute category rating is the method of subjective testing. The MOSs range from 1 to 5.
- **SPAQ [11]:** The SPAQ database consists of 11,125 in-the-wild pictures taken by 66 smartphones. Each picture is annotated with quality, attributes, and scene categories using the single-stimulus methodology. The MOSs range from 0 to 100.
- **AGIQA-3K [23]:** The AGIQA-3K consists of 2,982 AI-generated images derived from 6 advanced text-to-image generation models, which include AttnGAN [59], DALLE2 [39], GLIDE [37], Midjourney [17], Stable Diffusion [40], and Stable Diffusion XL [41]. The single-stimulus continuous quality rating is used to collect human opinions. The MOSs range from 0 to 5.
- **LIVE-Wild [12]:** The LIVE In the Wild (LIVE Challenge) database contains 1,162 authentically distorted images captured by diverse mobile devices in real-world conditions. The subjective testing method is large-scale crowdsourced continuous quality rating. The MOSs range from 0 to 100.
- **PIPAL [14]:** The PIPAL dataset contains 250 high-quality reference patches ( $288 \times 288$ ) sampled from DIV2K/Flickr2K and 29K distorted images generated from 40 distortion/processing types (including traditional distortions, restoration/SR outputs, and GAN-based results), with 116 distorted variants per reference. Subjective scores are collected via pairwise comparisons and aggregated using an Elo rating system. The MOSs are Elo-based scores (typically on the order of  $\sim 1000$ – $1800$ ).

## B Additional Qualitative Results.

The main results report aggregate correlation metrics across multiple benchmarks, while Fig. A provides additional qualitative comparisons. Across diverse content, Q-Tacit, Q-Insight [25], and VisualQuality-R1 [58] are prompted with the default rating query. Within each row, the three images are derived from the same source image but processed with different degradation settings (from KADID-10k [27]), resulting in a graded quality change with corresponding normalized MOS annotations. This controlled setup enables a direct assessment of relative score behavior: Q-Tacit’s predictions track the MOS trend more closely within each row, whereas text-space baselines (Q-Insight and VisualQuality-R1) exhibit relative bias, over- or underestimating particular variants. Q-Tacit more consistently preserves the MOS ordering among subtly different variants in these examples. These qualitative observations complement the main quantitative results by illustrating how the latent space supports consistent score ordering and stable per-image predictions.

## C Model Complexity Comparison.

Table A compares the computational footprint of representative reasoning-based IQA methods under a unified setting (input resolution  $512 \times 384 \times 3$ ). By leveraging a compact latent reasoning segment, Q-Tacit achieves a favorable trade-off: it significantly reduces inference time relative to text-space reasoning baselines and lowers TFLOPs compared to Q-Insight/VisualQuality-R1, demonstrating the improved efficiency of compact tokens.

Q: What is your overall rating on the quality of this picture?

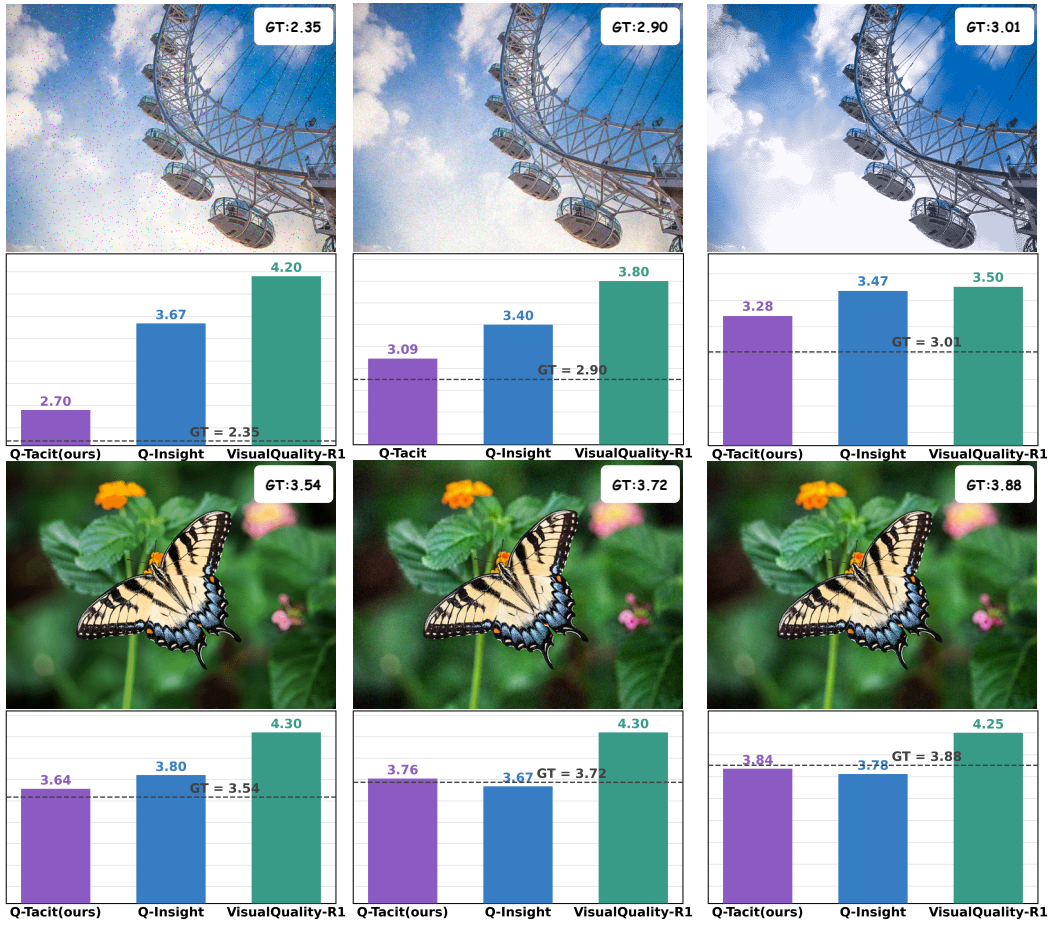


Figure A: **Qualitative score prediction examples from KADID-10k [27]**. For each example, the normalized MOS as ground-truth score (GT) is shown above the image, and the bar plot compares predicted scores from Q-Tacit, Q-Insight [25], and VisualQuality-R1 [58]. The dashed line indicates GT for easier visual comparison.

Table A: Averaged model complexity comparison using  $512 \times 384 \times 3$  images as input tested on single GH200 GPU.

Method	#Parameters	Inference Time ↓	Inference Memory	#TFLOPs ↓
Q-Insight [25]	8.29 B	2.22 s	15.6 G	8.13
VisualQuality-R1 [58]	8.29 B	2.04 s	15.6 G	7.49
<b>Q-Tacit(Ours)</b>	8.29 B	0.83 s	15.6 G	6.62